

## Prediction of ions migration behavior in mortar under 2-D ALMT application to inhibit ASR

Chih-Chien Liu<sup>1</sup> and Wen-Ten Kuo<sup>\*2</sup>

<sup>1</sup>Department of Civil Engineering, ROC Military Academy, No.1, Wei-Wu Rd., Fengshan District, Kaohsiung 83059, Taiwan, R.O.C

<sup>2</sup>Department of Civil Engineering, National Kaohsiung University of Applied Sciences, No. 415, Chien-Kung Rd., Sanmin District, Kaohsiung 80778, Taiwan, R.O.C

(Received March 18, 2014, Revised July 1, 2014, Accepted July 6, 2014)

**Abstract.** This study investigated four electric field configurations of two-dimensional accelerate lithium migration technique (ALMT), including line-to-line, plane-to-line, contour-to-line and plane-to-plane, and analyzed the ion migration behavior and efficiency. It was found that the free ion distribution diagram and voltage distribution diagram were similar, and ions migrated in the power line direction. The electrode modules were used for the mortar specimen with w/c ratio of 0.5. The effectively processed areas accounted for 14.1%, 39.0%, 49.4% and 51.4% of total area respectively on Day 28. Larger electrode area was more advantageous to ion migration. In addition, it was proved that the two-dimensional electric field could be divided into different equipotential line active regions, and regarded as affected by one-dimensional electric field, and the ion migration results in various equipotential line active regions were predicted by using the duration analysis method based on the theoretical model of ion migration obtained from one-dimensional test.

**Keywords:** electrochemical; alkali-silica reaction; ALMT; lithium

---

### 1. Introduction

The alkali-silica reaction (ASR) is the most extensively distributed alkali aggregate reaction (AAR) type damaging the structures most severely at present (Ueda *et al.* 2013, Beyene *et al.* 2013, Donnella *et al.* 2013, Gao *et al.* 2013, Demir and Arslan 2013, Yurtdas *et al.* 2013, Bach *et al.* 2013). It occurs after the hydration of cement, and the concrete pore solution contains free ions of Na<sup>+</sup>, K<sup>+</sup>, Ca<sup>2+</sup> and OH<sup>-</sup>. If the concrete contains ASR reactive aggregate, the OH<sup>-</sup> breaks the silicon-oxygen bonding with lower bond energy on the surface of reactive aggregate to generate negatively charged -Si-O<sup>-</sup>. It combines positively charged cation into steady product. The Na<sup>+</sup> and K<sup>+</sup> carry monovalent cation and are smaller than Ca<sup>2+</sup>, so they are more likely to be combined into stable alkali-silica gel. The swelling capacity of sodium-silica gel and potassium-silica gel is higher than that of calcium-silica gel. This gel expands when it absorbs water, so that the concrete has failure by bulging (Liu 2003).

---

\*Corresponding author, Professor, E-mail: [wtkuo@cc.kuas.edu.tw](mailto:wtkuo@cc.kuas.edu.tw)

For fresh concrete, the ASR prevention methods include limiting the alkali content in concrete, using non-reactive aggregate, adding mineral admixtures such as fly ash, silica fume or slag, or adding chemical admixture containing Li compound. Hobbs used opal as aggregate, and indicated the concrete specimen had no expansion reaction when the total alkali content in concrete was less than  $2 \text{ kg/m}^3$  (Hobbs 1984). Due to the difference in aggregate reactivity, the total alkali content limits for inhibiting ASR are different in different countries, for example, it is  $3.3 \text{ kg/m}^3$  in the U.S.,  $5.5 \text{ kg/m}^3$  in New Zealand,  $2 \text{ kg/m}^3$  in Australia,  $2.1 \text{ kg/m}^3$  in South Africa, and  $3 \text{ kg/m}^3$  in Canada (Ghanem *et al.* 2010). In addition, the recommended addition for effective inhibition is Li/(Na+K) molar ratio greater than 0.74 (Michael *et al.* 2007).

The waterproofing engineering can be used for hardened concrete. However, Daidai *et al.* indicated that the cracks in the concrete piers of a bridge built in 1972 were filled up with epoxy in 1989, and coated with waterproof layer (Daidai and Torii 2008). However, 5 years later, the protective layer had obvious cracks, the bridge was finally demolished and rebuilt for severe internal damage. Another strategy is to feed  $\text{Li}^+$  in for long-term inside improvement. If lithium solution is used for soaking, the  $\text{Li}^+$  only penetrates into the surface (Folliard *et al.* 2008). If pressurization is adopted, the  $\text{Li}^+$  penetrates a short distance, taking a long time, and the effect is inconsistent (Era *et al.* 2008). The penetration distance can be increased, and the required time can be reduced by applying electric field to feed  $\text{Li}^+$  into the concrete (Liu 2003, Liu *et al.* 2011).

The ALMT uses electric characteristics to feed  $\text{Li}^+$  into the concrete while accelerating removing  $\text{Na}^+$  and  $\text{K}^+$  out of concrete, so as to solve the ASR problem thoroughly (Liu 2003, Liu *et al.* 2011, Wang 2010, Wang *et al.* 2011, Wang 2014). At present, the research findings of ALMT construct the effect of one-dimensional electric field and obtain the theoretical model and empirical equation of ion migration (Liu *et al.* 2011). As the one-dimensional ALMT can process limited practical problems, the influence of the electrode configuration of two-dimensional electric field on the migration behavior of cations related to ASR still needs to be discussed.

This study discussed four probable electric field configurations of two-dimensional ALMT, including line-to-line, plane-to-line, contour-to-line and plane-to-plane, and analyzed the ion migration behavior and efficiency of mortar specimen (Liu *et al.* 2013). The two-dimensional electric field was divided into different equipfield line active regions in the concept of equipfield line, regarded as affected by one-dimensional electric field. The theoretical model of ion migration obtained from one-dimensional ALMT test was used to evaluate the feasibility of using duration analysis method to predict the ion migration behavior in various equipfield line active regions (Liu *et al.* 2011).

## 2. Experimental design

Four two-dimensional electrode forms may be used in the practical application of ALMT: line-line, plane-line, plane-plane and contour-line. This study applied the concept of equipfield line in the two-dimensional electric field to draw equipfield line, and then marked different one-dimensional equipfield affected subregions. The empirical equation of  $\text{Na}^+$  and  $\text{K}^+$  migration in one-dimensional electric field obtained from Wang (Liu *et al.* 2011) test and the duration analysis were used to calculate

the ion feed and emigration quantity in different subregions of equipfield line, and to estimate the ion content distribution under the effect of two-dimensional electric field. The estimation result

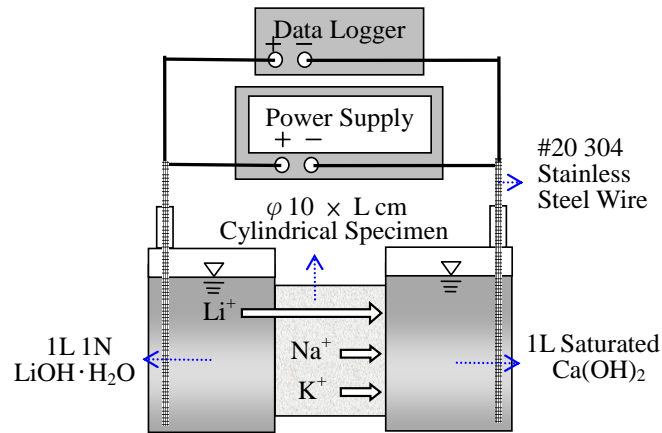


Fig. 1 One-dimensional ALMT schematic diagram

Table 1 Chemical composition of cement (%)

Item	SiO <sub>2</sub>	Al <sub>2</sub> O <sub>3</sub>	Fe <sub>2</sub> O <sub>3</sub>	CaO	MgO	SO <sub>3</sub>	F. CaO	K <sub>2</sub> O	Na <sub>2</sub> O	Na <sub>2</sub> O <sub>eq</sub>	I.L.
Result	20.65	3.85	3.66	63.83	3.38	2.18	0.65	0.52	0.18	0.52	1.17

was compared with the test result to validate the feasibility of using the ion migration characteristics of one-dimensional electric field in two-dimensional equipfield line to evaluate the ion migration behavior.

Fig. 1 shows the one-dimensional ALMT schematic diagram for applying a constant current density. Only the necessary exhaust openings were kept during the electrolysis process to prevent air dissolving into the electrolyte and increasing the resistance. A data logger was used to record changes in voltage or current, an ion chromatograph (IC) was used to analyze the cation concentration inside the cathode electrolyte, periodically, while the temperature changes within the cathodic cell were measured manually.

### 2.1 Specimen design and electrifying analysis method

The specimens of four electrode forms were made of mortar. The distance between electrode centers was 15 cm, the specimen was 15 cm in width and 5 cm in height. The line electrode was a circle in diameter of 2.5 cm, and the depth was 4 cm. The mix design of mortar was identical with that of Wang (Liu *et al.* 2011). The aggregate-cement ratio was fixed at 2.25, and the aggregate gradation distribution referred to ASTM C227 requirement. Three water-cement ratios were designed: 0.4, 0.5 and 0.6. The alkali equivalent in cement was adjusted from 0.52% to 2.0% by NaOH. The aggregate was river sand from western Taiwan, and it was metasandstone. Table 1 shows the chemical composition of cement. The form was removed on the following day, and then cured at 23°C, 100% R.H. for 3 months.

The specimen for measuring the voltage is shown in Fig. 2. Horizontal and vertical lines of 1.25 cm were marked on the mortar specimen. An iron nail was inserted in the center point of grid to measure the voltage inside the specimen. The voltage value was entered in the mapping software to draw isopotential line and equipfield line.

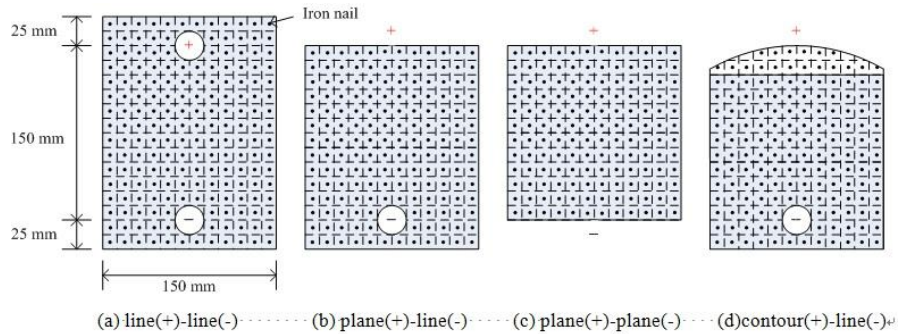
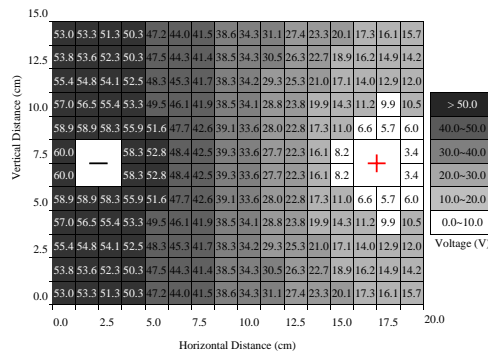
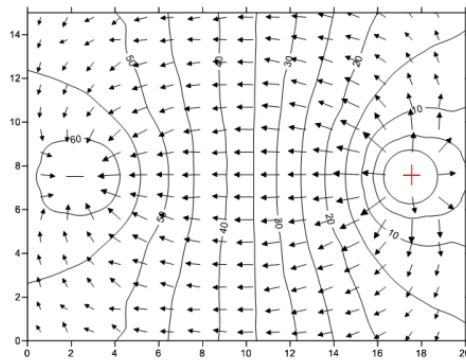


Fig. 2 Schematic diagram of mortar electrode module with iron nail inserted



(a) Recorded voltage



(b) Drawing isopotential line and equipotential line by Surfer 9 program

Fig. 3 Description of drawing method of isopotential line and equipotential line (take mortar specimen with w/c ratio of 0.5 as an example)

The electrifying module for ALMT test is shown in Fig. 2 without iron nail inserted. The applied current density was  $18 \text{ A/m}^2$  when the line electrode was anode. The applied current density was  $9 \text{ A/m}^2$  when the plane electrode was anode. The anode used 1 N LiOH solution, and the cathode used saturated  $\text{Ca(OH)}_2$  solution. The power-on time was 28 days. The line electrode was stainless steel bar, and the plane-contour electrode was a stainless steel mesh covered with

Table 2 Changes in voltage and resistance of various electrified modules

Electrode Configuration	W/C Ratio	Current Density (A/m <sup>2</sup> )	Initial Voltage (V)	Final Voltage (V)	Altered Voltage (%)	Passing Current (A)	Initial Resistance (Ω)	Final Resistance (Ω)	Altered Resistance (%)
line-line	0.4	18	124.0	74.6	-39.8	0.057	2175.4	1308.8	-39.8
	0.5		96.9	43.3	-55.3	0.054	1794.4	801.9	-55.3
	0.6		75.0	58.9	-21.5	0.054	1388.9	1090.7	-21.5
plane-line	0.5	9	90.7	114.5	26.2	0.069	1314.5	1659.4	26.2
plane-plane			67.6	123.5	82.7	0.069	979.7	1789.9	82.7
contour-line			89.5	108.4	21.1	0.071	1260.6	1526.8	21.1

cotton. The electrodes and solution were renewed every seven days in order to avoid the oxidation of anode on the stainless steel. In order to reduce the air that enters the cathode tank to form CO<sub>3</sub><sup>2-</sup> in the power on process, which may be combined with the Ca<sup>2+</sup> whose concentration increases gradually as the Na<sup>+</sup> and K<sup>+</sup> concentrations decrease inside the specimen at the final stage of electrifying to form CaCO<sub>3</sub> sediment blocking pores, the specimen was covered with preservative film in the entire process (Wu 2010).

When the specimen was electrified, a dry cut 1.25 × 1.25 × 1.25 cm specimen was studied. The water dissolution test was carried out referring to AASHTO T260. Taking 3 g of the sample (passing sieve #50) add 60 mL of deionized water into beaker. Heating the solution by the magnet heater until boiling, cool the solution after 5 minutes boiling and then standing for 24 hours. Filter the solution through CNS 5038G paper into beaker. Dilute the filtered solution. An Ion Chromatograph (IC) was used to analyze the free Li<sup>+</sup>, Na<sup>+</sup> and K<sup>+</sup> content distribution in the specimen.

### 2.1 Specimen design and electrifying analysis method

Fig. 2 shows the electrode setting. The power supply applied constant voltage. One end of digital multimeter was connected to the anode, and the other end was connected to the iron nail. The iron nail coordinates and voltage difference were recorded. The equipfield line was drawn by using Surfer 9 program according to the results. Surfer is a full-function 3D visualization, contouring and surface modeling package that runs under Microsoft Windows. Take line-to-line electrode as an example, Fig. 2 (a) is the schematic diagram of electrode electrifying, the measured voltage result is shown in Fig. 3(a). Fig. 3(b) shows the isopotential line and equipfield line.

## 3. Results and discussion

### 3.1 Voltage and resistance changes in electrifying

Table 2 shows the initial and final voltage and resistance changes in the course of electrifying of four electrode modules. The resistance of mortar specimen (Ω) = voltage (V)/current (A). The constant magnitude of current was applied in this study, so the resistance was proportional to voltage. In the ion migration process, the voltage dropped gradually at the initial stage of electrifying. As constant current was applied, the resistance of mortar specimen decreased

gradually. The anode area of line-line electrode module was small, the voltage dropped at the late stage of electrifying. The anode area of plane-line, plane-plane and contour-line electrode modules was large, thus, the applied voltage was increased in order to maintain constant magnitude of current at the late stage of electrifying. The resistance of specimen increases at the late stage of electrifying and the final voltage of plane-plane module increased the most.

The initial voltage was lower when the plane or contour was used as anode. The applied voltage increased gradually with the power on time, indicating that the resistance of mortar specimen increased. It might be due to the following reasons. First, the cations in the specimen migrated from the large-area anode to the small-area cathode, so the number of original  $\text{Na}^+$  and  $\text{K}^+$  ions in the specimen decreased in the mortar nearby the anode region at the late stage of electrifying. The quantity of  $\text{Ca}^{2+}$  dissolved out of  $\text{Ca}(\text{OH})_2$  increased, thus moving towards the cathode. Meanwhile, although the catholyte was sealed with preservative film in the course of electrifying, it was difficult to completely avoid the  $\text{CO}_2$  in the air dissolving in the catholyte to form  $\text{CO}_3^{2-}$  in the course of changing electrode, and it moved towards the anode, meeting with  $\text{Ca}^{2+}$  in the specimen to form  $\text{CaCO}_3$  blocking pores. Second, the anode was electrolyzed in the course of electrifying, and the formed metal ions were fed into the mortar under the effect of electric field. Literature (Wu 2010) showed that the resistance of mortar specimen increased under the influence mentioned above.

In addition, a lower water-cement ratio indicates less moisture in the concrete, denser structure, and fewer connected pore channels. In order to maintain a certain applied magnitude of current, higher voltage should be applied, so the initial voltage and average voltage increased as the water-cement ratio decreased.

### 3.2 Comparison between voltage distribution diagram and ion content distribution diagram

Fig. 4 shows the free cation distribution after the test of line-line electrode module of mortar specimen with w/c ratio of 0.4. For fresh concrete, two preventive strategies against ASR reactive aggregate can be adopted: (1) to control the  $\text{Na}_2\text{O}_{\text{eq}}$  content below  $3 \text{ kg/m}^3$ ; (2) to add Li compound to make the  $\text{Li}/(\text{Na}+\text{K})$  molar ratio higher than 0.74. This study measured the free cation content in mortar specimen. If the following two methods were used to identify the efficient processing region for preventing ASR: (1) the  $\text{Na}_2\text{O}_{\text{eq}}$  content should be controlled below  $3 \text{ kg/m}^3$ , if about 60% of it is free, the free value should be controlled below  $1.8 \text{ kg/m}^3$ ; or (2) if there is slight difference in the dissolution ratio of cations, the free  $\text{Li}/(\text{Na}+\text{K})$  molar ratio is higher than 0.74. The  $\text{Na}_2\text{O}_{\text{eq}}$  mortar specimen with water-cement ratio of 0.4 and alkali equivalent of 2.0 adopted line-to-line electrode module. The efficient processing region applied with  $18 \text{ A/m}^2$  on Day 28 of electrifying was within about 2.5 cm to the anode, accounting for 13.0% of the total area.

In the same way, for the specimens with w/c ratio of 0.5 and 0.6, the efficient processing regions were within about 3.75 cm and 8.75 cm to the periphery of anode respectively, as shown in Figs. 5 and 6, accounting for 14.1% and 33.7% of the total area, respectively.

The  $\text{Na}^+$  and  $\text{K}^+$  in the mortar migrated towards the cathode under the driving force of electric field, and the electric field intensity nearby two poles was large, as indicated by the arrow length in Fig. 3(b). The  $\text{Na}^+$  and  $\text{K}^+$  migrated from the anode towards the cathode in radiation form, as shown in Fig. 4(a). The  $\text{Li}^+$  in the anolyte was fed into the mortar in the same mode, and then migrated towards the cathode. In the calculation of distribution diagram of  $\text{Li}/(\text{Na}+\text{K})$  molar ratio

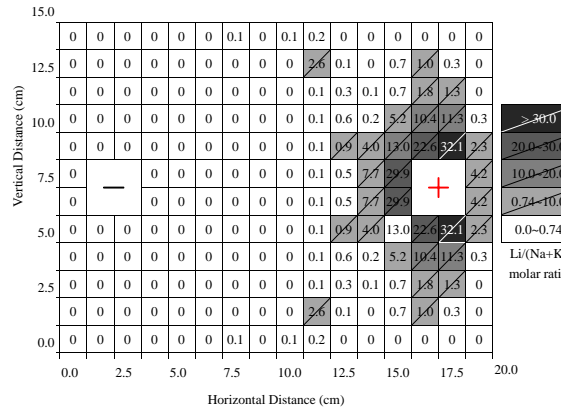
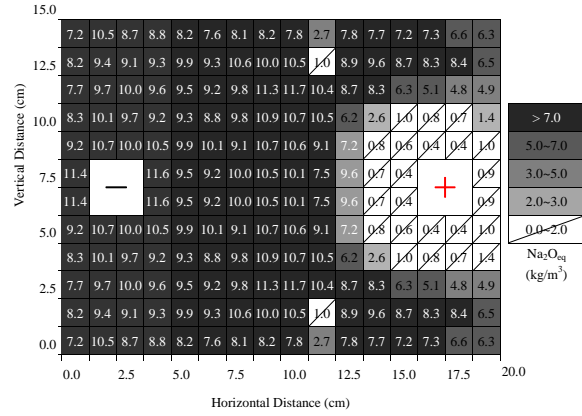


Fig. 4 Free cation distribution in line-to-line module (specimen with w/c ratio of 0.4)

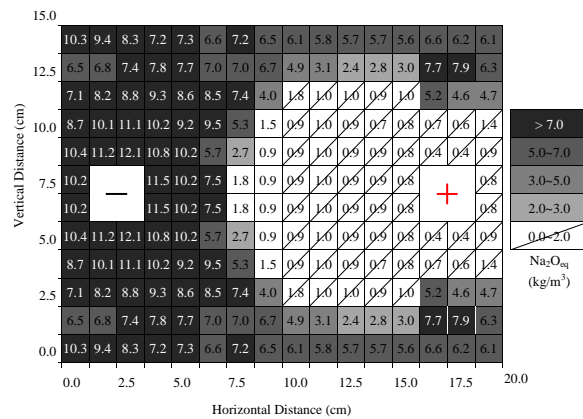
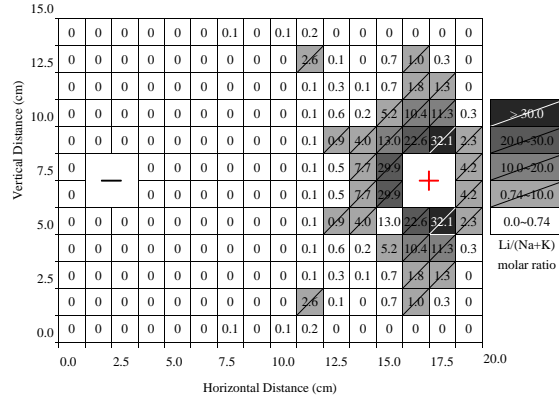
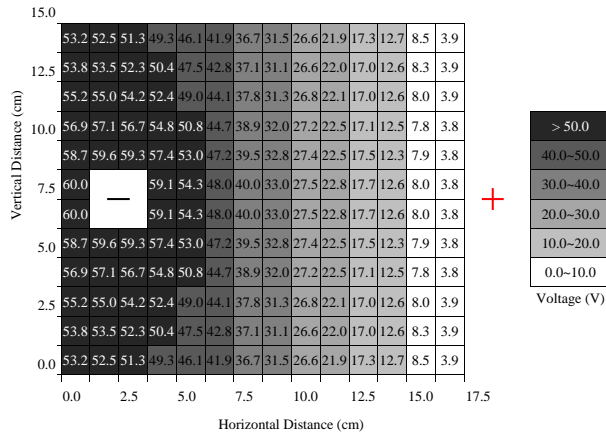


Fig. 6 Continued

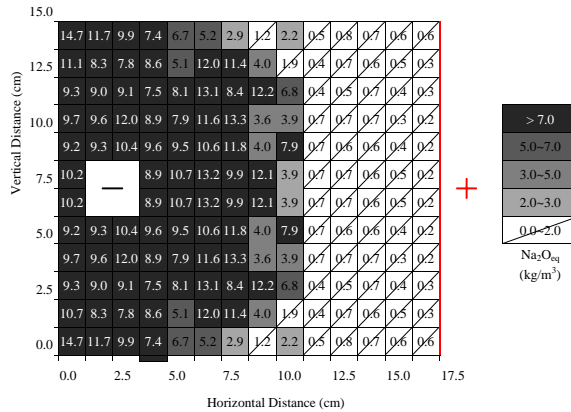


(b) Li/(Na+K) molar ratio

Fig. 6 Free cation distribution in line-to-line module (specimen with w/c ratio of 0.6)

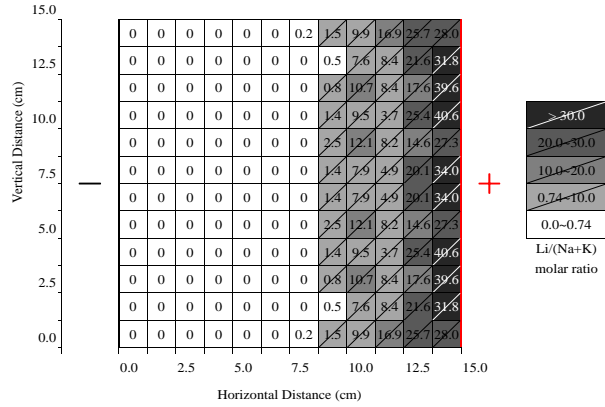


(a) Voltage



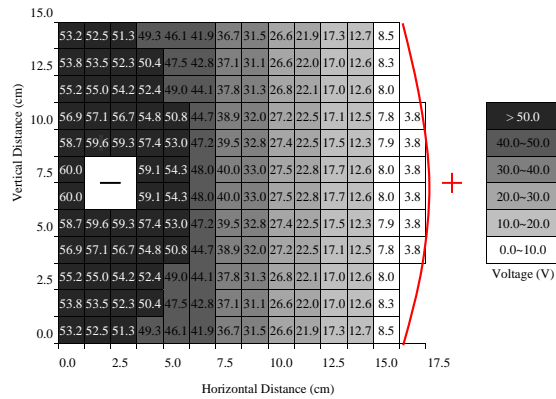
(b) Na<sub>2</sub>O<sub>eq</sub>

Fig. 7 Continued

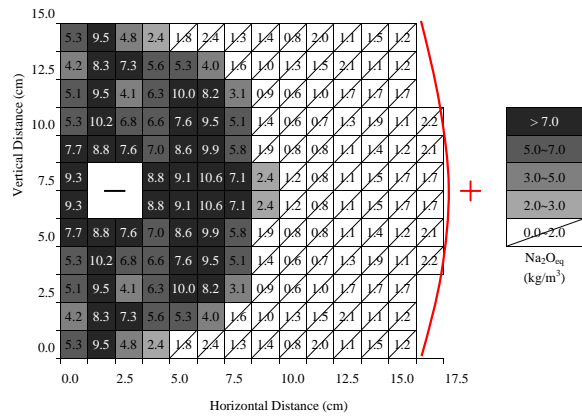


(c) Li/(Na+K) molar ratio

Fig. 7 Voltage and free cation distribution in plane-to-line module (specimen with w/c ratio of 0.5)

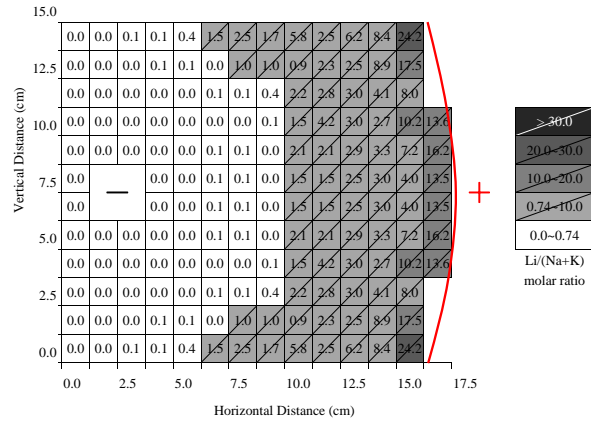


(a) Voltage



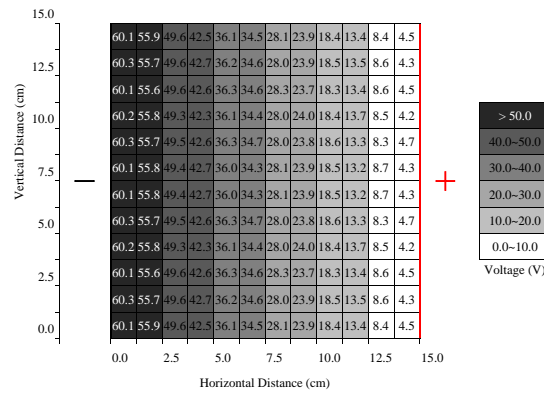
(b) Na<sub>2</sub>O<sub>eq</sub>

Fig. 8 Continued

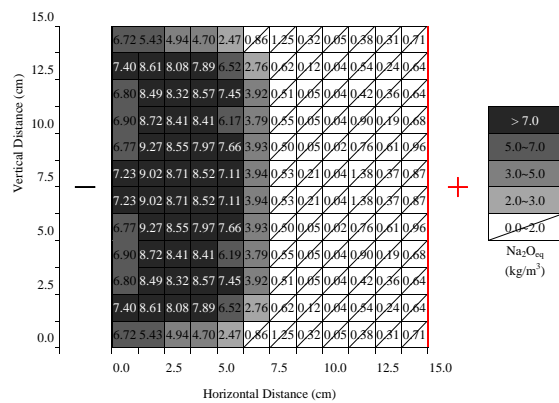


(c) Li/(Na+K) molar ratio

Fig. 8 Voltage and free cation distribution in contour-to-line module (specimen with w/c ratio of 0.5)

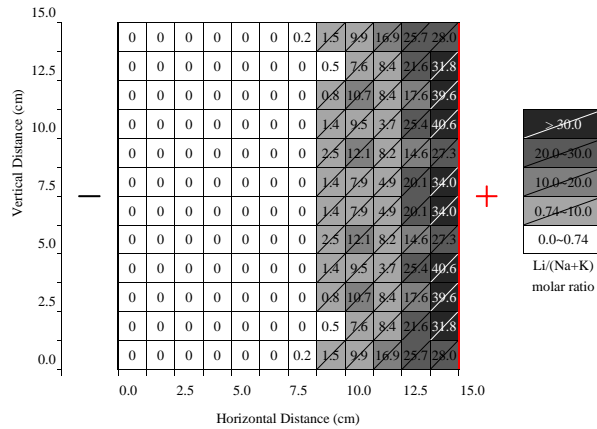


(a) Voltage



(b) Na<sub>2</sub>O<sub>eq</sub>

Fig. 9 Continued



(c) Li/(Na+K) molar ratio

Fig. 9 Voltage and free cation distribution in plane-to-plane module (specimen with w/c ratio of 0.5)

in mortar specimen, the  $\text{Li}^+$  migrated from the anode towards the cathode in radiation form, as shown in Fig. 4(b). The free total alkali content distribution diagram and the  $\text{Li}/(\text{Na}+\text{K})$  molar ratio distribution diagram in the electrified specimen were very similar to the voltage distribution diagram (Fig. 3(a)), the ions migrated in the power line direction.

Fig. 7 shows the voltage and free cation distribution in plane-to-line electrode test of mortar specimen with w/c ratio of 0.5. The region having alkals removed effectively was 7.5 cm away from the cathode border, as shown in Fig. 7(b). The region having  $\text{Li}^+$  fed in effectively was 10 cm away from the cathode border, as shown in Fig. 7(c), which matched the isopotential line distribution trend in Fig. 7(a). The efficient processing region accounted for 39.0% of the total area.

Fig. 8 shows the voltage and free cation distribution in contour-to-line electrode test of mortar specimen with w/c ratio of 0.5. The region having alkalis removed effectively was 7.5 cm away from the cathode border, as shown in Fig. 8(b). The region having  $\text{Li}^+$  fed in effectively was 7.5 cm away from the cathode border, as shown in Fig. 8(c), which matched the isopotential line distribution trend in Fig. 8(a). The efficient processing region accounted for 49.4% of the total area. Fig. 9 shows the voltage and free cation distribution in plane-to-plane electrode test of mortar specimen with w/c ratio of 0.5. The region having alkalis removed effectively was 7.5 cm away from the anode, as shown in Fig. 9(b). The region having  $\text{Li}^+$  fed in effectively was 6.25 cm away from the anode, as shown in Fig. 9(c), which matched the isopotential line distribution trend in Fig. 9(a). The efficient processing region accounted for 51.4% of the total area.

Fig. 9(b) shows that the residual free  $\text{Na}_2\text{O}_{\text{eq}}$  content at the upper and lower sides of specimen was lower. As shown in Fig. 9(c), the  $\text{Li}^+$  migrated faster at the upper and lower sides of specimen than in the middle part. The reason needed to be further studied.

According to the test of four probable electrode configuration modules, the ion migration path in the specimen was guided by the transmission of electric field. Therefore, isopotential line and equipfield line can be plotted when analyzing the ion migration behavior in two-dimensional ALMT test. The empirical equation of one-dimensional ALMT was used to estimate the ion migration for identical power transmission path. The feasibility of this idea will be analyzed in Section 3.3.

The applied electric field for plane and line electrodes is  $9 \text{ A/m}^2$  and  $18 \text{ A/m}^2$  and the electrode area for plane electrode is twice that of line electrode, so that all electrifying modules have the same accumulated electric quantity at the same electrifying duration. The same total electric quantity was applied to the mortar specimen in water-cement ratio of 0.5. According to the above test, for the line-to-line, plane-to-line, contour-to-line and plane-to-plane electrode modules, the effective processing regions accounted for 14.1%, 39.0%, 49.4% and 51.4% of the total area respectively. The result showed that larger electrode area is more advantageous to ion migration.

### 3.3 Estimate two-dimensional trial value using theoretical value of one-dimensional ALMT

According to the  $\text{Na}_2\text{O}_{\text{eq}}$  mortar specimen with w/c ratio of 0.5, ASTM C227 aggregate mix proportion with alkali content in cement of 2.0%  $\text{Na}_2\text{O}_{\text{eq}}$  in literature (Liu *et al.* 2011), under the effect of one-dimensional electric field, the  $\text{Na}^+$  removing velocity was  $0.019i$  ( $\times 10^{-3}$  mole/h), the  $\text{K}^+$  removing velocity was  $0.0048i$  ( $\times 10^{-3}$  mole/h), and  $i$  was the current density ( $\text{A/m}^2$ ).

As limited to the measurement of  $\text{Li}^+$  content, IC was used for analysis. Therefore, only the free cation content obtained from water dissolution could be measured, in order to compare the estimated value with the test value of theoretical value of two-dimensional ALMT test. The free form content of alkali metal ions inside the mortar specimen in the pore solution was analyzed first. It was found that the free  $\text{Na}^+$  and  $\text{K}^+$  contents accounted for 60% and 80% of the total contents of  $\text{Na}^+$  and  $\text{K}^+$  respectively.

If the line-line electrode module was used for analysis, the cathode and anode were divided into 16 equal parts by the isopotential line and equipfield line, as shown in Fig. 3. There would be 16 equipfield line regions. The Zone in Fig. 10(a) was analyzed as an example. This zone was divided into 10 subregions. Each subregion was regarded as affected by the one-dimensional electric field. The empirical equation of one-dimensional cation migration was used to calculate the total

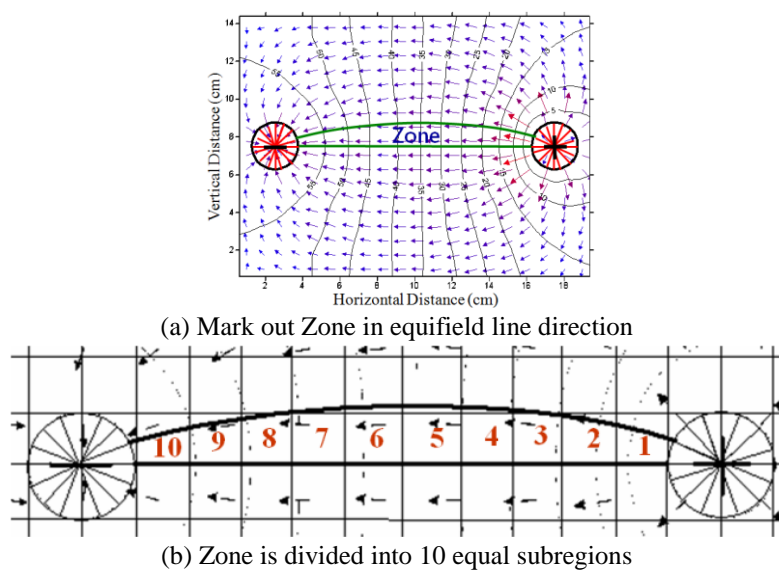


Fig. 10 Schematic diagram of equipfield line zoning

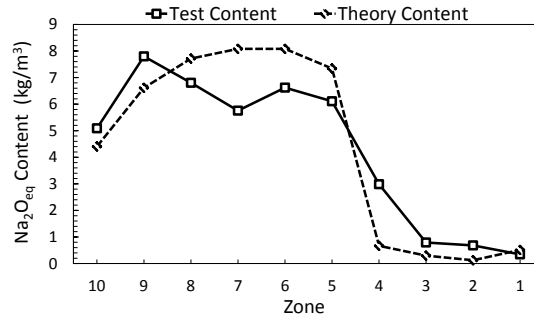


Fig. 11 Comparison of the prediction and test results of free quantity of  $\text{Na}_2\text{O}_{\text{eq}}$  in specimen with w/c ratio of 0.5 using line-to-line module

contents of initial free  $\text{Na}^+$  and  $\text{K}^+$  in each subregion. One day was a duration computing unit, the amount of movement of  $\text{Na}^+$  and  $\text{K}^+$  in the initial mortar specimen on Day 1 could be calculated by the given electric field intensity. The initial amount of each subregion at the beginning of electrifying on Day 2 could be obtained, then the initial amount on Day 3 could be obtained by calculating the amount of movement on Day 2, and so forth. The theoretical free residual quantity of  $\text{Na}^+$  and  $\text{K}^+$  in the mortar specimen on Day 28 of electrifying can be obtained.

The line-line electrified module was applied with  $18 \text{ A/m}^2$  constant current density in this study. The anode and cathode were in diameter of 2.5 cm, in depth of 4 cm, and the lateral surface area was  $0.002944 \text{ m}^2$ , so the applied rated current is 0.053 A. It was equally divided into 16 parts. The rated magnitude of current distributed to each part was 0.0033 A, namely, the current passing through Zone in Fig. 10 was 0.0033 A. The passed magnitude of current was divided by the average cross-section area of grids to obtain the average current density. The original  $\text{Na}^+$  and  $\text{K}^+$  contents in the mortar specimen in each subregion in Fig. 10(b) were calculated.

As the power on area of empirical equation was circular cross-section area in diameter of 10 cm, it should be converted into average sectional area of each specimen cube, so as to determine the actual removal velocity of ions. It was found that in the same electric field line, the current was identical, the cross-section areas were different, so that the current densities were different. However, the ion removal velocity was the same, the  $\text{Na}^+$  removal velocity in each subregion was  $1.92 \times 10^{-4}$  mole/day, and the  $\text{K}^+$  removal velocity was  $0.49 \times 10^{-4}$  mole/day.

Fig. 11 compares the prediction and test results of theoretical value of residual quantity of free  $\text{Na}_2\text{O}_{\text{eq}}$  in mortar specimen with w/c ratio of 0.5 using line-to-line electrode module. It was found that there is no significant difference between them, indicating that the two-dimensional electric field ALMT test can use the concept of equipfield line to divide two-dimensional electric field into different equipfield line active regions. For each equipfield line active region, the theoretical model of ion migration obtained from one-dimensional ALMT test was used to predict the result of ion migration using duration analysis method.

#### 4. Conclusions

This study discussed four probable electric field configurations of two-dimensional ALMT, and analyzed the ion migration in mortar specimen. The equipfield line concept was used to divide the

two-dimensional electric field into subregions under the effect of one-dimensional electric field. The theoretical equation of one-dimensional electric field was used to calculate the time-varying migration of ions, compared with test result. The conclusions are described below:

- The free total alkali content distribution diagram in electrified specimen and Li/(Na+K) molar ratio distribution diagram were very similar to voltage distribution diagram, the ions migrated in the power line direction.
- In terms of mortar specimen with w/c ratio of 0.5, for the line-to-line, plane-to-line, contour-to-line and plane-to-plane electrode modules, when the same total electric quantity was applied to the mortar specimen, the effective processing area accounted for 14.1%, 39.0%, 49.4% and 51.4% of the total area respectively. Larger electrode area was more advantageous to ion migration.
- The equifield line concept could be applied for ALMT test of two-dimensional electric field. The two-dimensional electric field was divided into different equifield line active regions, regarded as affected by one-dimensional electric field. The theoretical model of ion migration obtained from one-dimensional ALMT test was used to predict the ion migration in various equifield line active regions by using duration analysis method.

## Acknowledgements

The authors would like to thank the National Science Council of Taiwan for their financial support of this research under Contract No. NSC 100-2221-E-145-006.

## References

- ASTM C227, "Standard test method for potential alkali reactivity of cement-aggregate combinations (mortar-bar method)".
- AASHTO T260, "Standard method of test for sampling and testing for chloride ion in concrete and concrete raw materials".
- Bach, T.T.H., Chabas, E., Pochard, I., Coumes, C.C.D., Haas, J., Frizon, F. and Nonat, A. (2013), "Retention of alkali ions by hydrated low-pH cements: Mechanism and Na<sup>+</sup>/K<sup>+</sup> selectivity", *Cem. Concr. Res.*, **51**, 14-21.
- Beyene, M., Snyder, A., Lee, R.J. and Blaszkiewicz, M. (2013), "Alkali silica reaction (ASR) as a root cause of distress in a concrete made from alkali carbonate reaction (ACR) potentially susceptible aggregates", *Cem. Concr. Res.*, **51**, 85-95.
- Daidai, T. and Torii, K. (2008), "A proposal for rehabilitation of ASR-affected bridge piers with fractured steel bars", *Proceeding of the 13th International Conference on Alkali-Aggregate Reaction*, Trondheim, Norway, June.
- Demir, I. and Arslan, M. (2013), "The mechanical and microstructural properties of Li<sub>2</sub>SO<sub>4</sub>, LiNO<sub>3</sub>, Li<sub>2</sub>CO<sub>3</sub> and LiBr added mortars exposed to alkali-silica reaction", *Constr. Build. Mater.*, **42**, 64-77.
- Donnella, K.M., Zoughia, R. and Kurtisb, K.E. (2013), "Demonstration of microwave method for detection of alkali-silica reaction (ASR) gel in cement-based materials", *Cem. Concr. Res.*, **44**, 1-7.
- Era, K., Mihara, T., Kaneyoshi, A. and Miyagawa, T. (2008), "Controlling effect of lithium nitrite on alkali-aggregate reaction", *Proceeding of the 13th International Conference on Alkali-Aggregate Reaction*, Trondheim, Norway, June.
- Folliard, K.J., Thomas, M.D.A., Ideker, J.H., East, B. and Fournier, B. (2008), "Case studies of treating

- ASR-affected structures with lithium nitrate”, *Proceeding of the 13th International Conference on Alkali-Aggregate Reaction*, Trondheim, Norway, June.
- Gao, X.X., Multon, S., Cyr, M. and Sellier, A. (2013), “Alkali-silica reaction (ASR) expansion: Pessimism effect versus scale effect”, *Cem. Concr. Res.*, **44**, 25-33.
- Ghanem, H., Zollinger, D. and Lytton, R. (2010), “Predicting ASR aggregate reactivity in terms of its activation energy”, *Constr. Build. Mater.*, **24**(7), 1101-1108.
- Hobbs, D.W. (1984), “Expansion of concrete due to alkali-silica reaction”, *Struct. Eng.*, **62a**(1), 26-33.
- Liu, C.C. (2003), “Identify the reactivity of aggregates in Taiwan and using electrochemical techniques to mitigate expansion due to alkali-aggregate reaction in concrete”, Ph.D. Dissertation, National Central University, Jhongli. (in Chinese).
- Liu, C.C., Lee, C. and Wang, W.C. (2011), “Behavior of cations in mortar under accelerated lithium migration technique controlled by a constant voltage”, *J. Mar. Sci. Technol.*, **19**(1), 26-34.
- Liu, C.C., Kuo, W.T. and Huang, C.Y. (2013), “Equipfield line simulation and ion migration prediction for concrete under 2-D electric field”, *Comput. Concr.*, **12**(4), 431-442.
- Michael, D.A., Thomas, B.F., Kevin, J.F., Jason, H.I. and Yadhira, R. (2007), “The use of lithium to prevent or mitigate alkali-silica reaction in concrete pavements and structures”, Federal Highway Administration, U.S. Department Transportation, FHWA-HRT-06-133, 29-31.
- Ueda, T., Baba, Y. and Nanasawa, A. (2013), “Penetration of lithium into ASR-affected concrete due to electro-osmosis of lithium carbonate solution”, *Constr. Build. Mater.*, **39**, 113-118.
- Wang, W.C. (2010), “A study of using one dimensional electrochemical cation migration technique to inhibit concrete ASR”, Ph.D. Dissertation, National Central University, Jhongli. (in Chinese).
- Wang, W.C., Liu, C.C. and Lee, C. (2011), “Migration of cations in mortar under an electrical field controlled by a constant current density”, *Adv. Mater. Res.*, **150-151**, 362-372.
- Wang, W. C. (2014), “Effects of fly ash and lithium compounds on the water-soluble alkali and lithium content of cement specimens”, *Constr. Build. Mater.*, **50**, 727-735.
- Wu, S.C. (2010), “Accelerate lithium migration technique on the rebar and the bond strength”, Master thesis, National Central University, Jhongli. (in Chinese).
- Yurtdas, I., Chen, D., Hu, D.W. and Shao, J.F. (2013), “Influence of alkali silica reaction (ASR) on mechanical properties of mortar”, *Constr. Build. Mater.*, **47**, 165-174.